Large-Scale Controlled Synthesis of FeCo Nanocubes and Microcages by Wet Chemistry

Xian-Wen Wei,*,# Guo-Xing Zhu,# Yuan-Jun Liu,# Yong-Hong Ni,# You Song,‡ and Zheng Xu‡

College of Chemistry and Materials Science, Anhui Key Laboratory of Functional Molecular Solids, Anhui Normal University, Wuhu 241000, P. R. China, and State Key Laboratory of Coordination Chemistry, Coordination Chemistry Institute, Nanjing University, Nanjing 210093, P. R. China

Received February 22, 2008. Revised Manuscript Received July 21, 2008

Nanocubes and hollow cubic microcages of FeCo alloy have been synthesized in large scale by reduction of aqueous Fe^{2+} and Co^{2+} with hydrazine in the presence of poly(ethylene glycol) and cyclohexane at a relative low temperature, which were confirmed by X-ray powder diffraction, transmission electron microscopy, and scanning electron microscopy. The morphology and dimensions of FeCo alloy nanocrystals could be controlled by the reaction conditions such as the concentrations of cyclohexane and PEG-400, reaction time, and the molar ratio of Fe^{2+} to Co^{2+} in the solution. The concentration of iron in these particles could be varied between 17% and 56%. The highest magnetization of 211.9 emu/g was recorded for 68 ± 6 nm $Fe_{50}Co_{50}$ nanocubes. The work demonstrates that shape and size-controlled synthesis can offer a simple solution to fabricate magnetic FeCo nanocubes that are promising for single nanoparticle recording and for high performance exchange-spring nanocomposite magnetic applications.

Introduction

Shape control of metal nanoparticles has received considerable attention in recent years because of the strong correlation between the morphology and the chemical, physical, electronic, optic, magnetic, and catalytic properties of a nanoparticle.[1] Magnetic FeCo alloys are usually soft-magnetic materials with high saturation magnetizations (up to 2.45 T), low magnetostriction, high resistivity, small coercive forces, high curie temperature, and high magnetic anisotropy energies (even higher than that of FePt by prediction)[2] and are very interesting for technical applications, e.g. in read-write heads of magnetic storage devices, electronic bearings, biotechnology,[3] high-temperature space powder systems,[2] and microactuators.[4] Therefore, many techniques such as radiofrequency plasma torch,[5] mechanical alloying,[6] electrodeposition,[7] chemical vapor deposition,[3b] thermolysis of cobalt and iron carbonyl in the presence of surfactant,[3c,8] and reduction of Fe^{2+} and Co^{2+} precursors with H_2 or a gas mixture of 93% Ar + 3% H_2 at 300 °C[9] or with sodium borohydride followed by crystallization[10] or

* To whom correspondence should be addressed. E-mail: xwwei@mail.ahnu.edu.cn, tel: 86-553-3937138, fax: 86-553-3869303.

Anhui Normal University.

‡ Nanjing University.

(1) (a) For example: Chen, S.; Wang, Z. L.; Ballato, J.; Foulger, S. H.; Carroll, D. L. *J. Am. Chem. Soc.* **2003**, *125*, 16186. (b) Wang, Z. L.; Ahmad, T. S.; El-Sayed, M. A. *Surf. Sci.* **1997**, *380*, 302. (c) Narayanan, R.; El-sayed, M. A. *J. Am. Chem. Soc.* **2004**, *126*, 7194. (d) Chen, J.; Herricks, T.; Xia, Y. N. *Angew. Chem., Int. Ed.* **2005**, *44*, 2589. (e) Peng, X. G.; Manna, L.; Yang, W.; Wickham, J.; Scher, E.; Kadavanich, A.; Alivisatos, A. P. *Nature* **2000**, *404*, 59. (f) Yamada, M.; Kon, S.; Miyake, M. *Chem. Lett.* **2005**, *34*, 1050. (g) Zheng, Y. H.; Cheng, Y.; Wang, Y. S.; Bao, F.; Zhou, L. H.; Wei, X. F.; Zhang, Y. Y.; Zheng, Q. *J. Phys. Chem. B* **2006**, *110*, 3093. (h) Sun, Y. G.; Xia, Y. N. *Adv. Mater.* **2003**, *15*, 695. (i) Zhang, J. G.; Gao, Y.; Alvarez-Puebla, R. A.; Buriak, J. M.; Fenniri, H. *Adv. Mater.* **2006**, *18*, 3233. (j) Lee, H.; Habas, S. E.; Kweskin, S.; Butcher, D.; Somorjai, G. A.; Yang, P. D. *Angew. Chem., Int. Ed.* **2006**, *45*, 7824.

(2) (a) Burkert, T.; Nordström, L.; Eriksson, O.; Heinonen, O. *Phys. Rev. Lett.* **2004**, *93*, 027203. (b) Zeng, H.; Li, J.; Liu, J. P.; Wang, Z. L.; Sun, S. *Nature* **2002**, *420*, 395. (c) Zeng, H.; Li, J.; Wang, Z. L.; Liu, J. P.; Sun, S. *Nano Lett.* **2004**, *4*, 187. (d) Sunder, R. S.; Deevi, S. C. *Int. Mater. Rev.* **2005**, *50*, 157.

(3) (a) Sun, S.; Zeng, H.; Robinson, D. B.; Raoux, S.; Rice, P. M.; Wang, S. X.; Li, G. *J. Am. Chem. Soc.* **2004**, *126*, 273. (b) Seo, W. S.; Lee, J. H.; Sun, X.; Suzuki, Y.; Mann, D.; Liu, Z.; Terashima, M.; Yang, P.; Mcconnell, M. V.; Nishimura, D. G.; Dai, H. *Nat. Mater.* **2006**, *5*, 971. (c) Behrens, S.; Bönnemann, H.; Matoussevitch, N.; Gorschinski, A.; Dinjus, E.; Habicht, W.; Bolle, J.; Zinoveva, S.; Palina, N.; Hormes, J.; Modrow, H.; Bahr, S.; Kempter, V. *J. Phys.: Condens. Matter* **2006**, *18*, S2543.

(4) Shang, C. H.; Weihs, T. P.; Cammarata, R. C.; Ji, Y.; Chien, C. L. *J. Appl. Phys.* **2000**, *87*, 6508.

(5) Turgut, Z.; Nuhfer, N. T.; Piehler, H. R.; McHenry, M. E. *J. Appl. Phys.* **1999**, *85*, 4406.

(6) (a) Brüning, R.; Samwer, K.; Kuhrt, C.; Schultz, L. *J. Appl. Phys.* **1992**, *72*, 2978. (b) Kuhrt, C.; Schultz, L. *J. Appl. Phys.* **1993**, *73*, 6588. (c) Fenineche, N. E.; Hamzaoui, R.; El Kedim, O. *Mater. Lett.* **2003**, *57*, 4165.

(7) (a) Manciera, V.; Delplanckea, J. L.; Delwiche, J.; Hubin-Franskin, M. J.; Piquer, C.; Rebbouh, L.; Grandjean, F. *J. Magn. Magn. Mater.* **2004**, *281*, 27. (b) Myung, N. V.; Park, D. Y.; Urgiles, D. E.; George, T. *Electrochim. Acta* **2004**, *49*, 4397. (c) Qin, D. H.; Cao, L.; Sun, Q. Y.; Huang, Y.; Li, H. L. *Chem. Phys. Lett.* **2002**, *358*, 484. (d) Vilain, S.; Ebothé, J. *Mater. Sci. Eng., C* **2001**, *15*, 199. (e) Basu, S.; Unruh, K. M.; Parvizi-Majidi, A.; Xiao, J. Q. *J. Appl. P hys.* **2000**, *87*, 5840. (f) Tanahashi, K.; Maeda, M. *J. Appl. Phys.* **1984**, *56*, 581. (g) Bai, A.; Hu, C. C. *Electrochem. Commun.* **2003**, *5*, 78.

(8) (a) Sudfeld, D.; Wojczykowski, K.; Hachmann, W.; Jutzi, P.; Reiss, G.; Hütten, A. *J. Appl. Phys.* **2003**, *93*, 7328. (b) Bonnemann, H.; Brand, R. A.; Brijoux, W.; Hofstadt, H.-W.; Frerichs, M.; Kempter, V.; Maus-Friedrichs, W.; Matoussevitch, N.; Nagabhushana, K. S.; Voigts, F.; Caps, V. *Appl. Organomet. Chem.* **2005**, *19*, 790.

(9) (a) Desvaux, C.; Amiens, C.; Fejes, P.; Renaud, P.; Respaud, M.; Lecante, P.; Snoeck, E.; Chaudret, B. *Nat. Mater.* **2005**, *4*, 750. (b) Chaubey, G. S.; Barcena, C.; Poudyal, N.; Rong, C.; Gao, J.; Sun, S.; Liu, J. P. *J. Am. Chem. Soc.* **2007**, *129*, 7214.

(10) Zoriasatain, S.; Azarkharman, F.; Sebt, S. A.; Akhavan, M. *J. Magn. Magn. Mater.* **2006**, *300*, 525.

10.1021/cm800518x CCC: $40.75
Published on Web 09/10/2008

with polyols[11] have been applied toward the production of FeCo alloy nanostructures. Normally these syntheses are expensive (costly reagents or high energy cost) and involved difficulties in controlling size and morphology, and the resultant nanostructures are often spherical or lack well-defined facets, which is important for a catalytic reaction by nanostructures.[12] Wang et al. synthesized FeCo nanocubes[13] by a dc magnetron cosputtering deposition followed with online heating at 730 °C, and then the FeCo nanocube was coated by a thin Au shell with a nanocluster deposition technique directly from the gas phase.[14] Very recently Jeyadevan et al. also obtained FeCo nanodice in ethylene glycol at 403 K.[11c] However, it is still a challenge to prepare FeCo nanocubes with well-defined facets by a large-scale, facile, easy controlled, and energy-conserving manner, although Co nanocubes,[15] Fe nanocubes[16] by the reaction of $Fe[N(SiMe_3)_2]_2$ with H_2, and FePt nanocubes[17] by simultaneous decomposition of $Fe(CO)_5$ and reduction of $Pt(acac)_2$ have been achieved, and many other metal such as Pt,[18] Ag,[19] Pd,[20] Au,[21] Cu,[22] Ge,[23] and Bi[24] nanocubes or quasi-nanocubes have also been reported.

Herein we report an alternative new wet chemical route to FeCo nanocubes and hollow cubic microcages in large-scale by reduction of aqueous Fe^{2+} and Co^{2+} with hydrazine in the presence of poly(ethylene glycol) (PEG) and cyclohexane (C_6H_{12}). The work demonstrates that shape and size-controlled synthesis can offer a simple solution to fabrication of FeCo nanocubes with high saturation magnetization. Our procedure is conducted under a relative low temperature (78 °C) and requires no seed-mediated growth so that it is easier and more practical for large-scale synthesis.

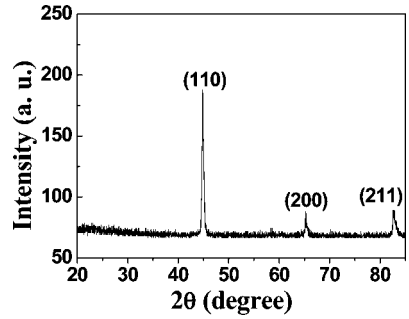

Figure 1. XRD pattern of FeCo nanostructures obtained by reaction of 0.1 M Fe^{2+} and Co^{2+} with hydrazine in the presences of 2.8 M PEG-400 and 0.14 M cyclohexane for 30 min.

Experimental Section

Sample Preparation. All chemicals used were of analytical grade and used as received without further purification. The typical procedure for sample 1 is as follows: Under argon atmosphere, 6.88 g of polyglycol (mw ≈ 400), 0.72 g of $FeSO_4 \cdot 7H_2O$, 0.64 g of $CoCl_2 \cdot 6H_2O$, and 0.8 mL of cyclohexane were in order dissolved in 50 mL of water. After being under ultrasonic radiation for 80 min at room temperature, the above mixture was heated to 78 °C and a solution composed of 20 mL of $NH_2-NH_2 \cdot H_2O$ (85 wt%) and 2.47 g of NaOH was added. After a reaction for 30 min, the final products were separated by centrifugation, washed five times with water, suspended in dry toluene and slightly oxidized to make them air stable, washed two times with acetone, and dried in vacuum at room temperature for 4 h. A 0.29 g amount of FeCo alloy in a yield of 95% was obtained. Using the same procedures, the concentrations of cyclohexane and PEG-400, time scale, and the molar ratio of metal precursors were varied in the experiments to obtain particles with a desired morphology, size, and composition.

Material Characterization. X-ray powder diffraction (XRD) was carried out on a Shimadzu XRD-6000 X-ray diffractometer with Cu Kα radiation ($\lambda = 1.54060$ Å) in the 2θ range from 20 to 85°. Transmission electron microscopy (TEM) micrographs were taken using a Hitachi H-800 transmission electron microscope, with an accelerating voltage of 200 kV. High-resolution TEM (HRTEM) was performed using JEM-2010 microscope operated at 200 kV. Magnetization was measured at room temperature using a BHV-55 vibrating sample magnetometer (VSM) and superconducting quantum interference device (SQUID) magnetometer. Scanning electron microscopy (SEM) images and energy-dispersive X-ray (EDX) spectra were recorded with a LEO-1350 VP field emission scanning electron microscope. Element analysis of Fe and Co was measured on an MFX-IF2 atomic absorption spectrophotometer.

Results and Discussion

Structural Analysis. Figure 1 shows the powder X-ray diffraction (XRD) pattern of the typical FeCo nanostructures obtained by reaction of 0.1 M Fe^{2+} and Co^{2+} with hydrazine for 30 min in the presences of 2.8 M PEG-400 and 0.14 M cyclohexane (sample 1, see Supporting Information (SI), SI-1), the peaks can be easily assigned to the (110), (200), and (211) reflections of the cubic FeCo alloy (JCPDS No. 49-1568), respectively.

In our synthesis system, the cobalt and iron salts were reduced by hydrazine hydrate in concentrated basic media,

(11) (a) Viau, G.; Fiévet-Vincent, F.; Fiévet, F. *J. Mater. Chem.* **1996**, *6*, 1047. (b) Kodama, D.; Shinoda, K.; Sato, K.; Sato, Y.; Jeyadevan, B.; Tohji, K. *IEEE Trans. Magn.* **2006**, *42*, 2796. (c) Kodama, D.; Shinoda, K.; Sato, K.; Konno, Y.; Joseyphus, R. J.; Motomiya, K.; Takahashi, H.; Matsumoto, T.; Sato, Y.; Tohji, K.; Jeyadevan, B. *Adv. Mater.* **2006**, *18*, 3154.
(12) Narayanan, R.; El-Sayed, M. A. *Nano Lett.* **2004**, *4*, 1343.
(13) Xu, Y. H.; Qiu, J. M.; Bai, J. M.; Judy, J. H.; Wang, J. P. *J. Appl. Phys.* **2005**, *97*, 10J305.
(14) Bai, J. M.; Wang, J. P. *Appl. Phys. Lett.* **2005**, *87*, 152502.
(15) Wang, Z. L.; Dai, Z. R.; Sun, S. H. *Adv. Mater.* **2000**, *12*, 1944.
(16) Dumestre, F.; Chaudret, B.; Amiens, C.; Renaud, P.; Fejes, P. *Science* **2004**, *303*, 821.
(17) (a) Chen, M.; Kim, J.; Liu, J. P.; Fan, H. Y.; Sun, S. H. *J. Am. Chem. Soc.* **2006**, *128*, 7132. (b) Shukla, N.; Liu, C.; Roy, A. G. *Mater. Lett.* **2006**, *60*, 995.
(18) (a) Ahmadi, T. S.; Wang, Z. L.; Henglein, A.; El-Sayed, M. A. *Chem. Mater.* **1996**, *8*, 1161. (b) Ahmadi, T. S.; Wang, Z. L.; Green, T. C.; Henglein, A.; El-Sayed, M. A. *Science* **1996**, *272*, 1924. (c) Ren, J.; Tilley, R. D. *J. Am. Chem. Soc.* **2007**, *129*, 3287. (d) Yamada, M.; Kon, S.; Miyake, M. *Chem. Lett.* **2005**, *34*, 1050.
(19) (a) Sun, Y. G.; Xia, Y. N. *Science* **2002**, *298*, 2176. (b) Im, S. H.; Lee, Y. T.; Wiley, B.; Xia, Y. N. *Angew. Chem.* **2005**, *117*, 2192. *Angew. Chem., Int. Ed.* **2005**, *44*, 2154. (c) Yu, D. B.; Yam, V. W. *J. Am. Chem. Soc.* **2004**, *126*, 13200. (d) Chen, J.; McLellan, J. M.; Siekkinen, A.; Xiong, Y. J.; Li, Z. Y.; Xia, Y. N. *J. Am. Chem. Soc.* **2006**, *128*, 14776.
(20) (a) Xiong, Y. J.; Wiley, B.; Chen, J. Y.; Li, Z. Y.; Yin, Y. D.; Xia, Y. N. *Angew. Chem.* **2005**, *117*, 8127. *Angew. Chem., Int. Ed.* **2005**, *44*, 7913. (b) Xiong, Y. J.; Chen, J. Y.; Wiley, B.; Xia, Y. N.; Yin, Y. D.; Li, Z. Y. *Nano Lett.* **2005**, *5*, 1237.
(21) (a) Jin, R. C.; Egusa, S.; Scherer, N. F. *J. Am. Chem. Soc.* **2004**, *126*, 9900. (b) Sau, T. K.; Murphy, C. J. *J. Am. Chem. Soc.* **2004**, *126*, 8648. (c) Seo, D.; Park, J. C.; Song, H. *J. Am. Chem. Soc.* **2006**, *128*, 14863.
(22) (a) Zhou, G. J.; Lu, M. K.; Yang, Z. S. *Langmuir* **2006**, *22*, 5900. (b) Wang, Y. H.; Chen, P. L.; Liu, M. H. *Nanotechnology* **2006**, *17*, 6000.
(23) Wang, W. Z.; Huang, J. Y.; Ren, Z. F. *Langmuir* **2005**, *21*, 751.
(24) Wang, W. Z.; Poudel, B.; Ma, Y.; Ren, Z. F. *J. Phys. Chem. B* **2006**, *110*, 25702.

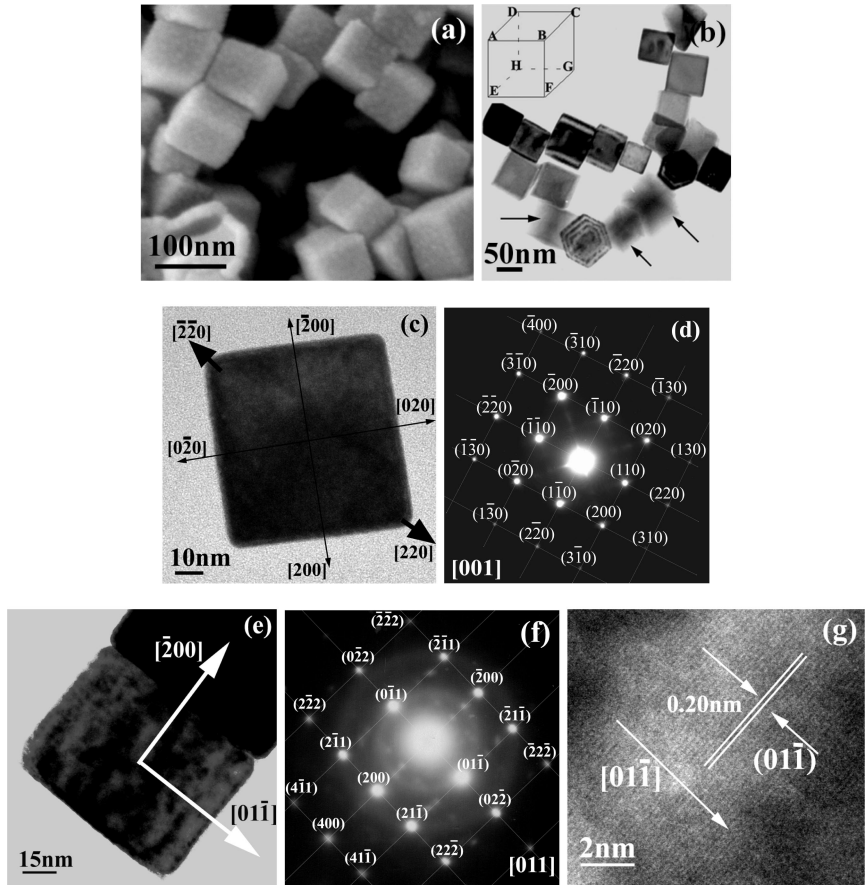

Figure 2. (a) SEM and (b) TEM micrographs of FeCo nanocubes, obtained by reaction of 0.1 M Fe^{2+} and Co^{2+} with hydrazine for 30 min in the presences of 2.8 M PEG-400 and 0.14 M cyclohexane. The inset is an illustration of the nanocube. (c) TEM image and (d) SAED pattern of a single FeCo alloy nanocube oriented along [001]. (e) TEM image, (f) SAED pattern, and (g) HRTEM image of a FeCo alloy nanocube oriented along [110].

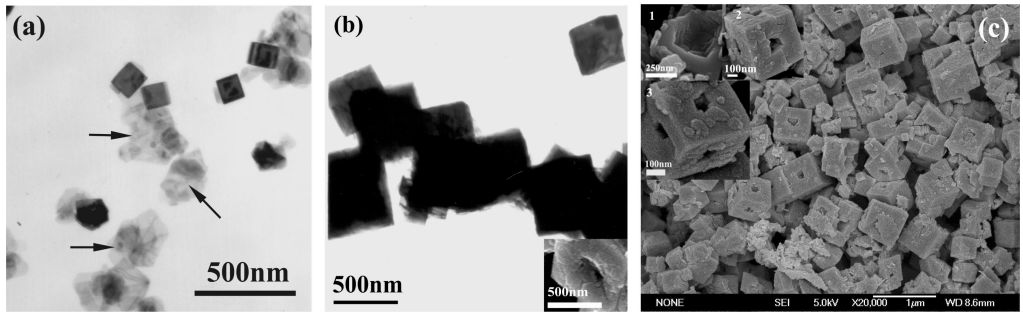

Figure 3. TEM and SEM micrographs of FeCo alloys prepared in the presence of (a) 0.28 M cyclohexane, (b) 0.28 M cyclohexane and 8.2 M PEG-400 (inset: SEM image of a microcube with holes), (c) 0.280 M cyclohexane and 16.4 M PEG-400 (inset: some magnified SEM images).

which can be explained by electromotive forces.[25] The reaction could be formulated as follows:

$$Co^{2+} + Fe^{2+} + N_2H_4 + 4OH^- \rightarrow FeCo + N_2 + 4H_2O \quad (1)$$

Morphology of FeCo Alloys. Figure 2a and 2b show scanning electron microscopy (SEM) and transmission electron microscopy (TEM) micrographs of a typical sample, respectively, indicated that the sample is composed of only FeCo alloy nanocubes with a mean edge length of 68 ± 6 nm. It is clear that the projection views of most particles are perfect square shapes and clear-cut edges. Some particles are self-aligned according to their magnetic dipolar interaction. Some particles are elongated and there is a transition of contrast along the direction of elongation (shown as the arrows) due to leaning on their cube edges. When leaning on vertexes, the projection was along the direction of BH (inset of Figure 2b), that is the [111] axis, and the view is hexagonal, as in the two nanocubes seen in Figure 2b.

Figure 2c shows a free-standing single nanocube. The corresponding selected-area electron diffraction (SAED) pattern (Figure 2d), indicating that the nanocube is a single crystal, is indexed to [001] zone of cubic FeCo alloy. The spots are indexed to {110} and {200} Bragg reflections,

(25) Su, X. B.; Zheng, H. G.; Yang, Z. P.; Zhu, Y. C.; Pan, A. L. *J. Mater. Sci.* **2003**, *38*, 4581.

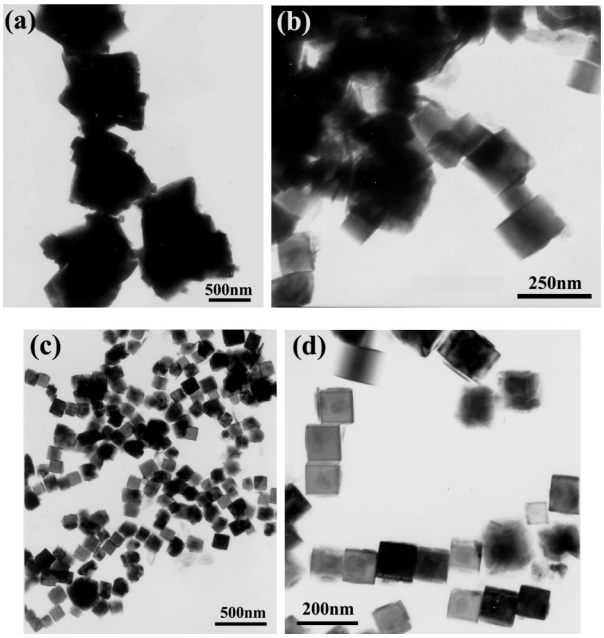

Figure 4. TEM micrographs of (a) 2-min, (b) 12-min, and (c, d) 90-min-growth FeCo nanocrystals obtained in the presence of 2.8 M PEG-400 and 0.14 M cyclohexane.

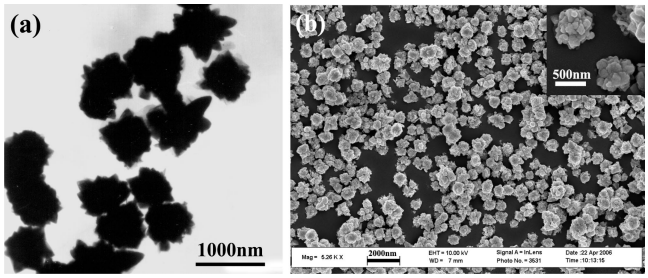

Figure 5. (a) TEM and (b) SEM micrograph of FeCo alloys obtained with $[Fe^{2+}]+[Co^{2+}] = 0.1$ M, $[Fe^{2+}]/[Co^{2+}] = 1/3$, 2.8 M PEG-400 and 0.14 M cyclohexane (the inset is a magnified SEM image).

while the corresponding SAED pattern (Figure 2f) of a nanocube leaning on its cube edge (Figure 2e) can be indexed to the [011] zone, which is the optimum orientation for imaging cubic structured materials. The high-resolution TEM (HRTEM) micrograph (Figure 2g) of the nanocube in Figure 2e shows that the nanocube is structurally single crystalline with a periodic fringe spacing of 0.20 nm, which corresponds to the interplanar spacing between the {110} planes of the cubic FeCo alloy. The thin oxidation shell with a thickness of about 3 nm caused by suspending the sample in dry toluene can also be seen from the HRTEM image (Supporting Information, SI-2). On the basis of the SAED and HRTEM images, it is known that each nanocube is abundant in crystallographic facets of {200} (shown in Figure 2c), which is similar to those reported face-centered cubic metal nanocubes.[18−22] The energy-dispersive X-ray (EDX) spectrum for a single nanocube indicates that it consists of FeCo with a composition of Fe (55.55 at. %) and Co (44.45 at. %) (Supporting Information, SI-3). The EDX spectrum for many FeCo nanocubes also gives similar composition ($Fe_{51.09}Co_{48.91}$). The average composition of the FeCo nanocubes was confirmed to be Fe:Co = 49.83:50.17 by atomic absorption spectrometry. All these indicate that the sample has a homogeneous composition, which is also similar to the original composition of Fe^{2+} and Co^{2+} in solution.

The morphology and dimensions of the product were found to strongly depend on reaction conditions such as the concentrations of cyclohexane and PEG-400, reaction time, and the molar ratio of Fe^{2+} to Co^{2+}. The cyclohexane and PEG-400 play important roles in the formation of FeCo nanocubes. Without cyclohexane and PEG-400, irregular $Fe_{50.4}Co_{49.6}$ nanoplates (containing little nanocubes) with ca. 100 nm (a few of about 200 nm) across and ca. 30 nm thick were obtained (Supporting Information, SI-4). When only 0.14 M of cyclohexane was present, a few FeCo nanocubes coexisted with FeCo nanoplates, and the situation was not changed with increasing the concentration of cyclohexane to 0.28 M, in which ca. 60% nanoplates existed (Figure 3a). When only 2.8 M of PEG-400 was used, FeCo nanocubes and some alloy nanorods (ca. 20%) with lengths of about 160 nm and diameters of about 12 nm coexisted (Supporting Information, SI-5). When 0.28 M of cyclohexane and 8.2 M or 16.4 M of PEG-400 were present, the microcubes (coexisted with some microcubic cages) or microcubic cages of $Fe_{43}Co_{57}$ with a mean edge length of 500 ± 150 nm were formed (Figure 3b, Figure 3c). Some of the microcubes in Figure 3b and almost all of the microcages in Figure 3c have holes in the middle of the six facets. When the concentration of cyclohexane was 0.026 M, varying the concentration of PEG-400 from 1.6 to 2.8 M, the morphology of FeCo changed from ca. 270 nm nanocubes to a mixture of nanorods and nanocubes (Supporting Information, SI-6). But only $CoFe_2O_4$ was obtained when the reaction was performed in the pure PEG-400, which means that the cobalt and iron salts were not reduced by hydrazine hydrate in the pure PEG-400. When 2.8 M PEG-400 was replaced by 3.0 M PEG-20000 or 0.064 M cetyltrimethylammonium bromide (CTAB), 83 ± 10 or 117 ± 20 nm FeCo nanocubes can also be obtained, respectively (Supporting Information, SI-7). Although agglomeration of the particles was evidenced in most of the samples, isolated particles could also be obtained.

The shape of a nanocrystal was mainly determined by the ratio of the growth rates of different crystallographic planes. The classic BFDH model[26] assumes the growth velocity (r_{hkl}) is inversely proportional to the interplanar spacing (d_{hkl}). For FeCo alloys, $d_{100} > d_{110} > d_{111}$, the growth rate sequence may hold $r_{111} > r_{110} > r_{100}$. The shape of a cubic nanocrystal was mainly determined by the ratio (R) between the growth rates along [100] and [111] directions. Perfect cubes bounded by the {100} planes will result if R is reduced to 0.58.[27] In our synthesis systems, PEG and cyclohexane, working in the presence of each other, may act as capped reagents and be adsorbed on the {100} planes, further decrease the growth rate of {100} planes, and lead to the cubic nanostructures

(26) Winn, D.; Doherty, M. F. *AIChE J.* **2000**, *46*, 1348.
(27) Wang, Z. L. *J. Phys. Chem. B* **2000**, *104*, 1153.

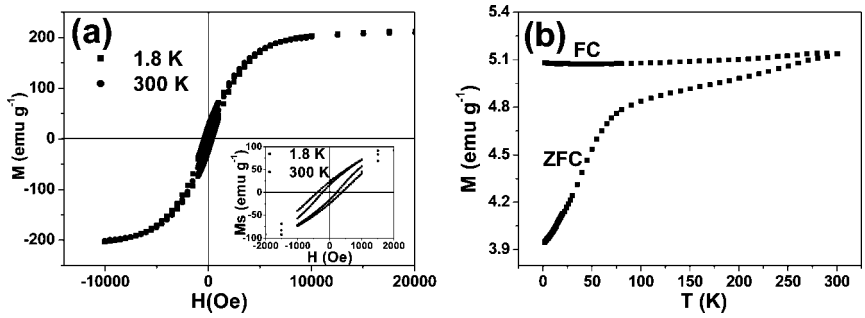

Figure 6. (a) Magnetic hysteresis loops at 1.8 and 300 K of $Fe_{50}Co_{50}$ alloy nanocubes (the inset is magnified hysteresis loops from −2000 to 2000 Oe) and (b) the corresponding ZFC-FC magnetization from 1.8 to 300 K.

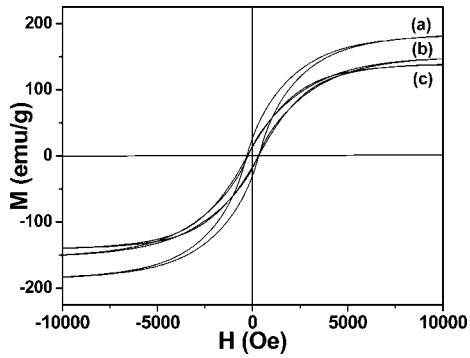

Figure 7. Room temperature magnetic hysteresis loops of FeCo alloy with (a) hollow cubic microcages obtained with 16.4 M PEG-400 and 0.28 M cyclohexane, (b) nanoplatelets obtained without cyclohexane and PEG-400, and (c) flower-like structures obtained with $[Fe^{2+}]+[Co^{2+}] = 0.1$ M, $[Fe^{2+}]/[Co^{2+}] = 1/3$, 2.8 M PEG-400 and 0.14 M cyclohexane.

enclosed by six {100} planes. The CTAB may have similar capping action[28] as PEG. The formation mechanism for $Fe_{43}Co_{57}$ microcages is intriguing and needs further study (Supporting Information, SI-8).

In order to study the growth mechanism of FeCo alloy nanocubes, we have monitored the crystalline growth process by collecting small portions (~0.5 mL) of the reacting mixture from time to time for TEM and XRD analyses. XRD indicated all of the crystals are cubic FeCo alloys. As the reaction time elapses from 2, 12, 30, to 90 min, the morphology of FeCo, as shown in Figure 4 and Figure 2, changed from polyhedron with a diameter of about 1000 nm and parts of small nanocubes, many nanocubes with an average diameter of about 94 nm and transitive morphology (polyhedron), to FeCo cubes with an average diameter of 68 ± 6 (Figure 2a,b) and 110 nm, respectively. These may reflect that the polyhedrons with big size are formed by kinetic control within a short reaction time, the small nanocubes gradually grow and the polyhedron decreases, and finally FeCo nanocubes are formed. Similar to PbSe nanocubes,[29] the driving force of the evolution from polyhedron to cubes may lie in the fact that the growth rate in the [100] direction is lower than other directions, although this type of growth results from various competitive factors such as crystalline size, growth temperature, the energy contributions from different parts of a crystal (such as interface, edges, and corners), and the kinetics.[30]

Keeping the total metal ion concentration constant, the morphologies and sizes of FeCo nano- or microcrystals are influenced by the molar ratio of Fe^{2+} to Co^{2+} in the original solutions. While the molar ratio of Fe^{2+} to Co^{2+} is 1:3, FeCo flower-like structures in a size of about 615 nm are obtained as shown in Figure 5. The EDX (Supporting Information, SI-9) for a single flower-like structure confirms that it consists of FeCo with an average composition of Fe (17.01 at. %) and Co (82.99 at. %), which is different from the original composition of Fe^{2+} and Co^{2+}. The content of Co in the outer part of flower-like structures (84.41 at. %) is higher than the center (81.43 at. %), indicating an inhomogeneous distribution of Fe and Co in alloys in this case. As the molar ratio of Fe^{2+} to Co^{2+} increased to 3:1, the product, characterized by XRD, is a mixture of FeCo alloys and oxides ($CoFe_2O_4$ or Fe_3O_4). The formation of Fe_3O_4 is maybe due to the oxidation of excessive metallic iron reduced by hydrazine during the course of the reaction and the relative lack of enough metallic cobalt in the system to form a more stable FeCo alloy phase. The corresponding TEM image of the sample (Supporting Information, SI-10) indicated that nanocubes and nanoparticles coexist. The observation that the morphology of FeCo was influenced by the molar ratio of Fe^{2+} to Co^{2+} further confirmed the concept that the crystal structure of the metal (body-centered cubic for Fe, hexagonal for Co) participates in the shape control of the mesoscopic nano-objects under thermodynamic conditions.[15] It has been reported that the shape of the FeCo particles varied from cubic to nearly spherical by the polyol reduction process when the particles were rich in Fe or Co, respectively, irrespective of the presence of poly(vinylpyrrolidine).[11c]

It should be noted that the cell constants of the FeCo alloys are calculated from the XRD pattern to be $a = 0.2842$, 0.2850, 0.2859 nm when the molar ratio of Fe^{2+} to Co^{2+} is 1:3, 1:1, 3:1, respectively. It is obvious that the cell constants increase with the decrease of the Co concentration, which is caused by the larger radius of the Fe atom (1.27 Å) compared to the Co atom (1.26 Å). When the Co atom enters the bcc structure of Fe-based alloys, the cell constants decrease. It has been reported that the Fe/Co composition could be easily controlled in the polyol reduction process. The FeCo particles with varying Fe

(28) Sun, Y.; Zhang, L. H.; Zhou, H. W.; Zhu, Y. M.; Sutter, E.; Ji, Y.; Rafailovich, M. H.; Sokolov, J. C. *Chem. Mater.* **2007**, *19*, 2065.
(29) Lu, W. G.; Fang, J.; Ding, Y.; Wang, Z. L. *J. Phys. Chem. B* **2005**, *109*, 19219.
(30) (a) Lee, S. M.; Jun, Y. W.; Cho, S. N.; Cheon, J. *J. Am. Chem. Soc.* **2002**, *124*, 11244. (b) Gabrisch, H.; Kjeldgaard, L.; Johnson, E.; Dahmen, U. *Acta Mater.* **2001**, *49*, 4259.

Table 1. Magnetic Data of Obtained FeCo Alloy Samples

samples	M_s (emu/g)	M_r (emu/g)	M_r/M_s	Hc (Oe)	M_s for bulk alloys with analogous compostion (emu/g)[6b]
$Fe_{43}Co_{57}$ microcubic cages (~500 nm, entry 6, Figure 3c)	180.2	28.0	0.16	311.1	212
$Fe_{50.4}Co_{49.6}$ nanoplatelets (~100 nm, entry 2, SI-4)	146.6	16. 4	0.11	266.5	225
$Fe_{17}Co_{83}$ flower-like structures (~615 nm, entry 10, Figure 5, SI-9)	137.2	14.9	0.11	297.0	186

concentration from 85% to 25% were synthesized by reacting a specific ratio (from 90:10 to 30:70) of Fe and Co salts (0.01 M) in ethylene glycol at 403 K for 1 h.[11c] However, in our synthesis system, the composition cannot be freely manipulated when the initial ratio of iron to cobalt ions is above 3:1 or less than 1:3, which is the same as that observed in the reduction of iron and cobalt ions with hydrazine hydrate in alcohol.[25]

Magnetic Property. The hysteresis loops of $Fe_{50}Co_{50}$ alloy cubes with a mean edge length of 68 ± 6 nm at 1.8 and 300 K (Figure 6a) show that the saturation magnetization (M_s), remanent magnetization (M_r), and coercivity (Hc) are 215.9 emu g^{-1}, 24.3 emu g^{-1}, and 380.7 Oe at 1.8 K, respectively, and 211.9 emu g^{-1}, 16.4 emu g^{-1}, and 219.2 Oe at 300 K, respectively. Figure 6b shows the temperature dependence of magnetization measured at 100 Oe from 300 to 1.8 K with a SQUID magnetometer. The fact that the curves are not superimposed at $T = 300$ K points out that the nanoparticles are still in the magnetic blocked state at this temperature. It is likely that blocking of nanoparticles is mainly due to high-strength dipolar interparticle magnetic interactions, as also suggested by the zero pendence of the FC curve[31] while the direct exchange interaction is unlikely due to the low probability of direct contact among the particles, as the presence of a thin oxide layer on the surface of nanocrystals.

Magnetic properties of other alloy samples with different shapes and compositions were also measured as shown in Figure 7. The M_s of all samples (the oxidation layers are not considered) are smaller than the highest M_s (245 emu/g) reported for the bulk $Fe_{65}Co_{35}$ alloy[9b,32] and that for the bulk FeCo alloy with analogous composition,[6b] although that of 68 ± 6 nm $Fe_{50}Co_{50}$ nanocubes (211.9 emu/g) is close to that value for the bulk $Fe_{50}Co_{50}$ alloy (225 emu/g).[6b] The surface spin disorder and oxidation are responsible for this phenomenon.[33] The M_r/M_s (0.11−0.16) have no big change among the samples, which indicates that the samples have a similar characteristic of an assembly of randomly oriented uniaxial particles.[34] The coercivities of all samples are much larger than that of bulk FeCo alloy with analogous composition (0.68 or 10−60 Oe),[35,6b] in which the reduced size may change the magnetization reversal mechanism, leading to a higher coercivity. The small difference of Hc among the samples may be mainly related to the different morphologies and thus a different shape anisotropy, since its variation closely follows the changes of morphologies. Certainly, this is not the only parameter that we have to consider. The composition, internal stress, defects, and size also influence this value.

Conclusions

In summary, FeCo alloy nanocubes in sizes of 60−270 nm and hollow cubic microcages have been synthesized in high yield and large-scale via a simple surfactant-assisted solution route. By controlling the concentrations of cyclohexane and PEG-400, the reaction time, and the initial molar ratio of Fe^{2+} to Co^{2+} in the solution, the morphology and dimensions of FeCo alloy nanocrystals have been manipulated. The cyclohexane and PEG-400 play important roles in the formation of FeCo nanocubes and microcages, which leads us to propose a growth mechanism. The magnetization of 68 ± 6 nm $Fe_{50}Co_{50}$ nanocubes is up to 211.9 emu/g, which is close to the value for the bulk material. The FeCo nanocubes may have important applications in catalytic reactions, medical diagnostics and therapies, single nanoparticle recording, and high performance exchange-spring nanocomposite magnets.

Acknowledgment. This work was supported by the Science and Technological Fund of Anhui Province for Outstanding Youth (No. 08040106906), the National Natural Science Foundation (Nos. 20671002, 20571002, 20490217, 20271002), the State Education Ministry (EYTP, SRF for ROCS, SRFDP20070370001) of P. R. China, and the Education Department (No. 2006KJ006TD) of Anhui Province.

Supporting Information Available: Typical conditions for the preparation of FeCo alloys; further characterization data for FeCo nanocubes and FeCo with different morphologies. This material is available free of charge via the Internet at http://pubs.acs.org.

CM800518X

(31) Casula, M. F.; Concas, G.; Congiu, F.; Corrias, A.; Falqui, A.; Spano, G. *J. Phys. Chem. B* **2005**, *109*, 23888.
(32) Liu, X. X.; Morisako, A. *J. Appl. Phys.* **2008**, *103*, 07E726.
(33) Kodoma, H. R.; Berkovitz, A. E., Jr.; Foner, S. *Phys. Rev. Lett.* **1996**, *77*, 394.
(34) Ung, D.; Viau, G.; Ricolleau, C.; Warmont, F.; Gredin, P.; Fiéver, F. *Adv. Mater.* **2005**, *17*, 338.
(35) Elías, A. L.; Rodríguez-Manzo, J. A.; McCartney, M. R.; Golberg, D.; Zamudio, A.; Baltazar, S. E.; López-Urías, F.; Muñoz-Sandoval, E.; Gu, L.; Tang, C. C.; Smith, D. J.; Bando, Y.; Terrones, H.; Terrones, M. *Nano Lett.* **2005**, *5*, 467.